Draft version March 4, 2009
Preprint typeset using LaTeX style emulateapj v. 10/09/06

arXiv:0903.0791v1 [astro-ph.SR] 4 Mar 2009

THREE-DIMENSIONAL NON-LTE RADIATIVE TRANSFER COMPUTATION OF THE CA 8542 INFRARED LINE FROM A RADIATION-MHD SIMULATION

J. Leenaarts[1], M. Carlsson[1] V. Hansteen[1], L. Rouppe van der Voort[1]
Institute of Theoretical Astrophysics, University of Oslo, P.O. Box 1029 Blindern, N-0315 Oslo, Norway
Draft version March 4, 2009

ABSTRACT

Interpretation of imagery of the solar chromosphere in the widely used Ca II 854.2 nm infrared line is hampered by its complex, three-dimensional and non-LTE formation. Forward modelling is required to aid understanding. We use a 3D non-LTE radiative transfer code to compute synthetic Ca II 854.2 nm images from a radiation-MHD simulation of the solar atmosphere spanning from the convection zone to the corona. We compare the simulation with observations obtained with the CRISP filter at the Swedish 1–m Solar Telescope. We find that the simulation reproduces dark patches in the blue line wing caused by Doppler shifts, brightenings in the line core caused by upward-propagating shocks and thin dark elongated structures in the line core that form the interface between upward and downward gas motion in the chromosphere. The synthetic line core is narrower than the observed one, indicating that the sun exhibits both more vigorous large-scale dynamics as well as small scale motions that are not resolved within the simulation, presumably owing to a lack of spatial resolution.

Subject headings: methods: numerical — Sun: atmosphere — Sun: chromosphere

1. INTRODUCTION

The solar chromosphere has traditionally been observed in the Ca II H&K and the Hα lines. The use of these lines as a diagnostic suffers from significant drawbacks. The Ca II H&K lines have wavelengths in the violet part of the spectrum. A trade-off has to be made between filter width and exposure time due to the lack of photons and the lower sensitivity of CCD chips at these wavelengths. Either the filter has to be wide, leading to significant low-chromospheric line wing contributions, or the long exposure time leads to lower spatial resolution due to difficulties with the image restoration (e.g. Lites et al. 1999; Wöger et al. 2006). In addition, the Ca II H&K lines are subject to partial redistribution (PRD), which complicates proper modeling of these lines.

Observations in the Hα line suffer to a much lower extent from these effects, but Hα line formation is very complex and proper modeling requires non-equilibrium ionization of hydrogen to be taken into account, physics that so far has only been treated in detail in one-dimensional (1D) models (Carlsson & Stein 2002).

These problems are much less severe for the Ca II 854.2 nm line. Non-equilibrium and PRD effects are less important for its formation (Uitenbroek 1989). Observations can be done with narrow filters and short exposure times, yielding a clean and high resolution view of the chromosphere. This makes it an excellent diagnostic, both from the observational as the modeling point-of-use, albeit at a lower diffraction-limited resolution than the Ca II H&K and the Hα lines.

Fabry-Pérot instruments such as IBIS (Cavallini 2006) and CRISP (Scharmer et al. 2008) now routinely observe the Ca II 854.2 nm line with high spectral, spatial, and temporal resolution. However, interpretation of data obtained with these instruments is non-trivial; forward modeling by computation of synthetic filtergrams from radiation-MHD simulation is needed to gain insight in the formation of the line.

The formation of the Ca II 854.2 nm line has been studied by Uitenbroek (2006) in the 1D semi-empirical FALC model (Fontenla et al. 1993) and the 1D dynamic models of Carlsson & Stein (1999) and a 3D snapshot of convection by Asplund et al. (2000). The 3D model did not include magnetic fields and extended up to 1 Mm above $\tau_{500} = 1$, lower than the formation height of the line core in the FALC model (see Fig. 5 of Cauzzi et al. 2008). In this paper we present synthetic images of the Ca II 854.2 nm line computed with a 3D non-LTE radiative transfer code from a snapshot of a radiation-MHD simulation that extends from the convection zone to the corona, capturing the whole height range of formation of the line.

2. OBSERVATIONS

Figure 3 shows observations in the Ca II 854.2 nm line obtained with the CRISP imaging spectropolarimeter (Scharmer et al. 2008) at the Swedish 1–m Solar Telescope. The data was obtained on June 13, 2008 and was taken at disk-center in a coronal hole. A scan through the line was made using 24 filter positions from -0.92 to $+0.19$ Å with a FWHM of the filter of 110 mÅ. The image quality was improved by post-processing using the MOMFBD algorithm (van Noort et al. 2005).

3. RADIATIVE TRANSFER COMPUTATION

The radiative transfer computation was based on a snapshot computed with the Oslo Stagger Code (Hansteen et al. 2007). This code employs an LTE equation of state and includes non-LTE radiative losses using a multi-group opacity method and thin radiative cooling in the corona and upper chromosphere. It includes thermal conduction along magnetic field lines. The simulation had $256 \times 128 \times 160$ grid points, corresponding

Electronic address: jorritl@astro.uio.no
[1] also at Center of Mathematics for Applications
University of Oslo, P.O. Box 1053 Blindern, N-0316 Oslo, Norway

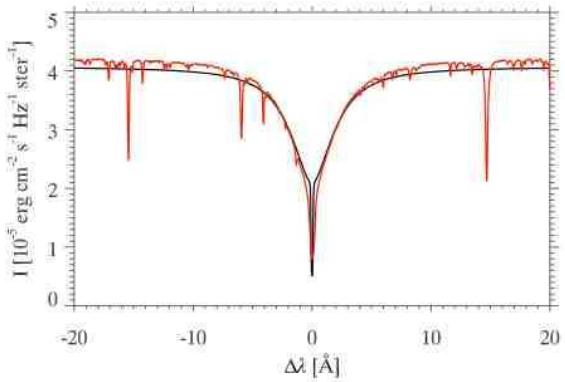

FIG. 1.— Average profile of the Ca 8542 IR line. Solid red: FTS atlas; solid black: simulation. The simulated continuum has a lower intensity and the line core is narrower than in the observed profile.

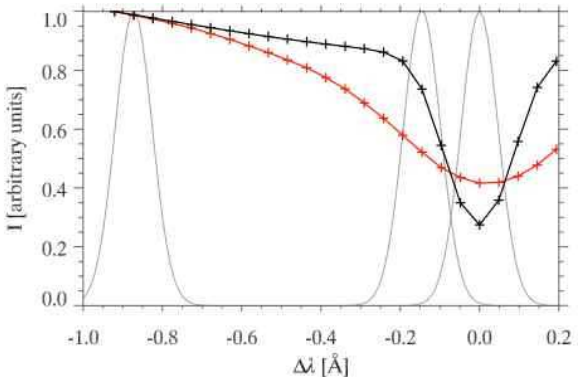

FIG. 2.— Line core of the Ca 8542 IR line. The profiles have been normalized on their values at $\Delta\lambda = -0.92$ Å. Solid red: CRISP; solid black: simulation; plus signs indicate the different filter positions. The gray curves show the shape and positions of the filter used to produce the synthetic images in Fig. 3. The synthetic line core is narrower than the observed one.

to a physical size of $16.6 \times 8.3 \times 15.5$ Mm. The snapshot has an averaged unsigned magnetic field strength of 150 G and covers a height range from 1.5 Mm below the photosphere up to 14 Mm above it, spanning from the upper convection zone up into the corona. For the radiative transfer computation the grid was interpolated onto a grid with 213 points in the z-direction covering a height range between -0.5 and 5.3 Mm relative to $\tau_{500} = 0$. The Ca II model atoms consists of 5 bound levels plus a continuum with 5 lines (Ca II H&K and the infrared triplet) and 5 bound-free transitions. The Ca II 854.2 nm line had 200 frequency points. All lines were computed in complete redistribution. Velocity fields were taken into account and no additional microturbulence was added. The electron density was computed assuming LTE ionization for all relevant species. Photoionization by hydrogen Lyman lines was not taken into account. The ray quadrature was computed using the A2 set of Carlson (1963). The radiative transfer computation was performed using an MPI-parallelized, domain-decomposed code named MULTI3D. This code is based on the 1D code MULTI (Scharmer & Carlsson 1985) and includes the same physics, but has a 3D short-characteristics formal solver, allowing evaluation of the 3D radiation field.

4. RESULTS

Figure 1 compares the average quiet sun profile of the Ca II 854.2 nm line from the FTS atlas (Neckel & Labs 1984) to the average profile computed from the simulation. The simulated continuum is 3.5% less bright than the observations, the line wings fit rather well, while the line core is narrower and the bisector does not show the inverse-C shape of the observations.

The vertically emergent intensity in the Ca II 854.2 nm line was convolved with the CRISP filter transmission function. Figure 2 compares the observed and synthetic profile averaged over the simulation box and a quiet region of the same size in the observations (shown in Fig. 3). The synthetic profile has a less steep inner wing and a narrower line core.

Figure 3 compares a quiet sun region from the observations to the synthetic filtergrams. The left panels show reversed granulation with several magnetic bright points. The contribution function in the upper-left panel of Fig. 4 shows that the intensity in the magnetic bright points are formed deeper than in the surrounding low-field-strength atmosphere, similar to G band bright points (Carlsson et al. 2004).

The middle panels of Fig. 3 show the atmosphere as seen in the "knee" of the line, where the profile changes from the LTE wings to the non-LTE formed line core (Cauzzi et al. 2008). Because of the difference in the line widths in the simulations and the observations this is at different offsets relative to line center, at -0.39 Å for the observations and -0.14 Å for the simulations. Nevertheless, they show a remarkably similar scene. The bright background shows the upper photosphere and lower chromosphere at around $z = 0.5$ Mm where the reversed granulation pattern changes to one dominated by acoustic shock interference (Wedemeyer et al. 2004).

The upper-middle panel of Fig. 3 shows black structures, for example at $(15, 1)$ and at $(15.5, 13)$ Mm. Similar roundish or thin elongated structures appear in the synthetic image. The corresponding contribution function panel in Fig. 4 shows that they are formed at around $z = 1.5$ Mm, 1 Mm higher than the bright background. Comparison with the lower right panel shows that the dark patches are associated with upflows and the line profile in Fig. 5 shows a blueshifted line at the positions of the dark patches.

There are three brightenings along the cut in the lower middle panel of Fig. 3, at $x = 1$, $x = 9.5$ and $x = 15.5$ Mm, all located above a photospheric magnetic field concentration (middle right panel of Fig. 4).

The right panels show the line core. The simulated image has a higher contrast, which can at least partly be explained by the fact that the observations are not corrected for scattered light. The observations show an amorphous background with a number of brightenings, such as at $(x, y) = (3.5, 3.5)$ and $(16, 8)$ Mm. They are often, but not always, located on top of or near bright points in the photosphere. The simulated line core image (lower right) shows similar brightenings, for example at $(x, y) = (1, 3)$ Mm. Fig. 4 shows that this brightening is associated with a strong downflow above a magnetic element. This brightening is formed much deeper than is the intensity along the rest of the cut. A similar brightening at $(x, y) = (9.5, 1.5)$ Mm is not associated with a photospheric magnetic field concentration, however. The corresponding line profile in Fig. 5 shows an emission peak slightly bluewards of line-center and an

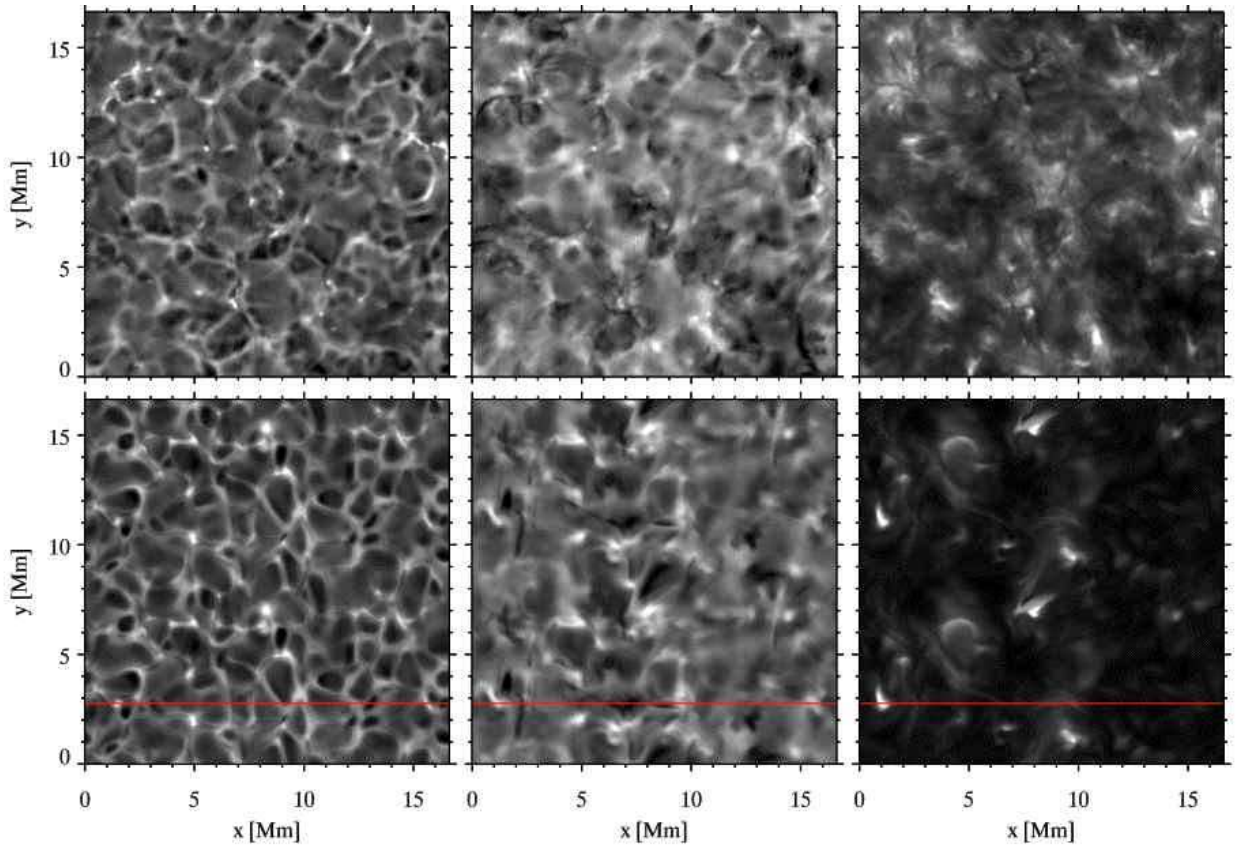

FIG. 3.— Observed (top row) and synthetic (bottom row) Ca II 854.2 nm images at different positions in the line. Left: at $\Delta\lambda = -0.87$ Å; middle: in the "knee" of the line, for the observations at $\Delta\lambda = -0.39$ Å and for the synthetic image at $\Delta\lambda = -0.14$ Å; right: in the line core at $\Delta\lambda = 0$ Å. The brightness scales are clipped at the brightest and darkest 0.1% of the pixels. The observed and synthetic images show similar structure in all panel pairs. The wavelengths of the middle panel pair are in the "knee" of the line profile, and because of the difference in the line core width this is not at the same wavelength. The red line indicates the cut displayed in Figs. 4 and 5.

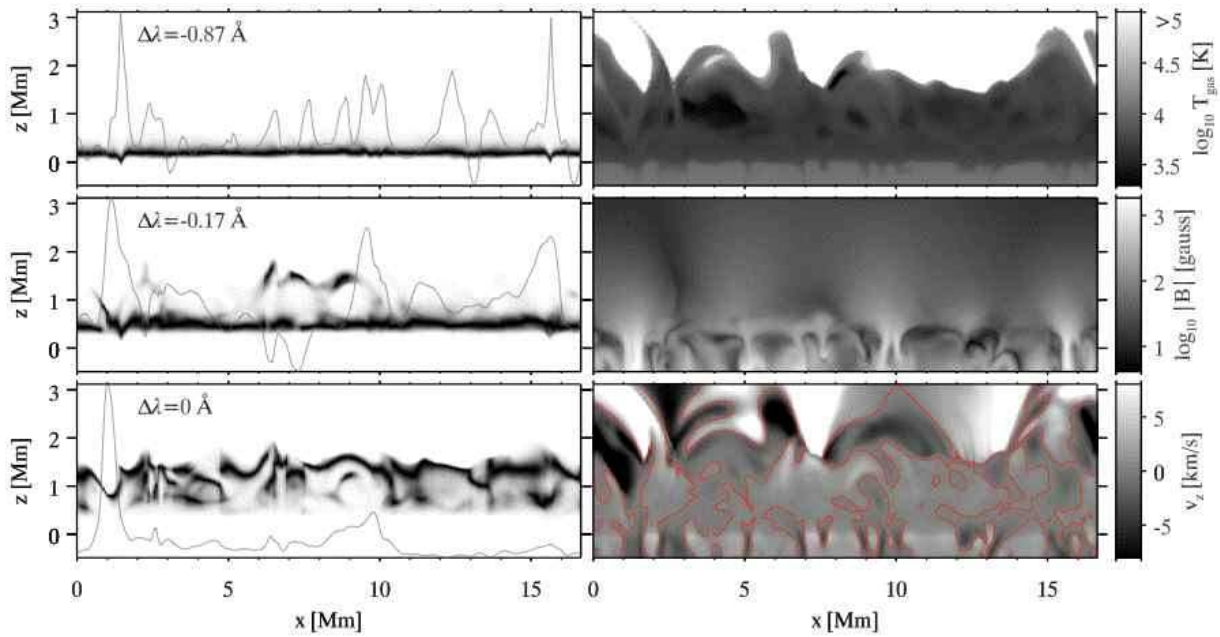

FIG. 4.— Vertical cut through the atmosphere along the red line in Fig. 3. The left-hand panels show the contribution function to the intensity within the CRISP filter, on an inverted brightness scale and with each column scaled to maximum contrast for improved visibility. The overplotted grey curves indicate the emergent intensity in arbitrary units. The right-hand panels show, from top to bottom, the gas temperature, the absolute magnetic field strength and the vertical velocity (positive means upflow). The red curve in the velocity panel indicates the zero vertical velocity contour.

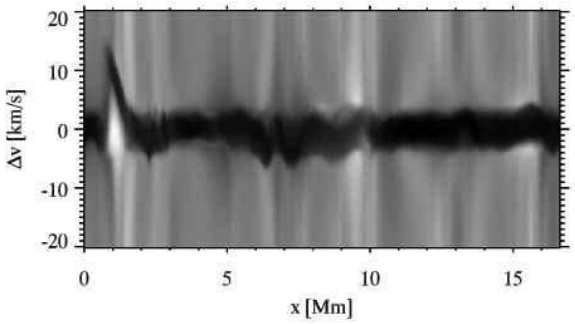

FIG. 5.— Emergent spectrum of the Ca II 854.2 nm line along the cut indicated in Fig. 3, with positive velocity corresponding to a redshift. The brightening at $(x, y) = (1, 3)$ Mm in the lower right panel of Fig. 3 is associated with a 12 km/s redshift of the line core. The dark patches between $y = 5$ and $y = 10$ Mm along the cut in the lower middle panel of Fig. 3 are associated with a blueshift of 5 km/s

intensity dip on the red side of the line typical of an upward propagating wave with downflowing material above it (see Carlsson & Stein 1997, for a detailed description in the case of the Ca II H2V grains). These shocks can be either acoustic or magneto-acoustic, the radiative transfer mechanism causing them to be bright in the line core remains the same, and a single snapshot alone is not sufficient to distinguish between them. Analysis of a time-series is needed to determine the wave type.

On top of the background in the upper right panel of Fig. 3 one can see filamentary dark structures that can be both straight and curved. They are mainly concentrated in the top left part of the image, but can be found throughout the field of view. The simulated line-core image shows similar dark filamentary structures (for example at $(x, y) = (2.5, 3)$ and $(10, 6)$ Mm). They appear similar to the observed ones, but tend to be straighter, though a slightly curved example can be found at $(x, y) = (4, 5)$ Mm. They are the interface between a patch of upflowing and downflowing material. They form where the vertical velocity at their formation height is zero and the line core is located at the rest frequency of the line. On either side of the dark filament the gas is moving up or down, shifting the line core to the blue or red and thus showing the brighter line wings at the rest frequency.

5. DISCUSSION & CONCLUSIONS

The simulation reproduces a number of observed features rather well, but there are a number important differences that carry large diagostic potential.

The difference in the continuum intensities in Fig. 1 can be explained by a small difference in the effective temperature of the simulation and the sun combined with the effect of box oscillations in the simulation, which causes fluctuations in the continuum intensity with an amplitude of about 1%.

The simulated spatially-averaged line-core profile is narrower than the observed one (Fig. 2). We computed the deviations of the position of the line core from the rest-wavelength over the field-of-view for both the simulation and the observation. The standard deviation for the simulations is 1.1 km/s, which is 50% smaller than for the observations. This indicates that the solar chromosphere has more vigorous large-scale dynamics than the simulation. However, this effect is too small to explain the difference in average line-core width.

We also inspected the line-core widths for individual resolution elements. The simulated line cores are on average narrower than the observed ones. This is the dominant reason for the difference in the average core width, indicating that the sun is dynamic on scales not resolved by the simulation.

Close inspection of the line core images of Fig. 3 shows that the observations have more structure on scales of about 0.1 Mm than the simulation, also hinting that the simulation does not have sufficient resolution to generate enough small-scale motion to broaden the line core.

In summary, we have computed the 3D, non-LTE, emergent intensity in the Ca II 854.2 nm line from a snapshot of a radiation-MHD simulation. It reproduces a number of observed features rather well, i.e., black patches in the blue 'knee' of the line, and thin dark lines and brightness enhancements in the line core. However, the simulated line core is narrower than the observed one, indicating that the sun shows more vigorous large scale dynamics and motions at smaller scales than can be resolved in the simulation. We intend to repeat the same analysis with a radiation-MHD simulation with higher spatial resolution.

J. Leenaarts is supported by the European Commission funded Research Training Network SOLAIRE. This research was supported by the Research Council of Norway through grant 170935/V30 and a grant of computing time from the Program for Supercomputing. The Swedish 1-m Solar Telescope is operated on the island of La Palma by the Institute for Solar Physics of the Royal Swedish Academy of Sciences in the Spanish Observatorio del Roque de los Muchachos of the Instituto de Astrofísica de Canarias.

REFERENCES

Asplund, M., Nordlund, Å., Trampedach, R., & Stein, R. F. 2000, A&A, 359, 743
Carlson, B. G. 1963, Methods of Computational Physics, Vol. 1
Carlsson, M. & Stein, R. E. 1999, in AIPC Series, 23
Carlsson, M. & Stein, R. F. 1997, ApJ, 481, 500
Carlsson, M. & Stein, R. F. 2002, ApJ, 572, 626
Carlsson, M., Stein, R. F., Nordlund, Å., & Scharmer, G. B. 2004, ApJ, 610, L137
Cauzzi, G., Reardon, K. P., Uitenbroek, H., et al. 2008, A&A, 480, 515
Cavallini, F. 2006, Sol. Phys., 236, 415
Fontenla, J. M., Avrett, E. H., & Loeser, R. 1993, ApJ, 406, 319
Hansteen, V. H., Carlsson, M., & Gudiksen, B. 2007, in ASPC Series, Vol. 368, 107
Lites, B. W., Rutten, R. J., & Berger, T. E. 1999, ApJ, 517, 1013
Neckel, H. & Labs, D. 1984, Sol. Phys., 90, 205
Scharmer, G. B. & Carlsson, M. 1985, J. Comput. Phys., 59, 56
Scharmer, G. B., Narayan, G., Hillberg, T., et al. 2008, ApJ, 689, L69
Uitenbroek, H. 1989, A&A, 213, 360
Uitenbroek, H. 2006, ApJ, 639, 516
van Noort, M., Rouppe van der Voort, L., & Löfdahl, M. G. 2005, Sol. Phys., 228, 191

Wedemeyer, S., Freytag, B., Steffen, M., Ludwig, H.-G., & Holweger, H. 2004, A&A, 414, 1121
Wöger, F., Wedemeyer-Böhm, S., Schmidt, W., & von der Lühe, O. 2006, A&A, 459, L9